Available online at www.sciencedirect.com
SCIENCE DIRECT®
International Journal of Mass Spectrometry 232 (2004) 249–258
International Journal of Mass Spectrometry
www.elsevier.com/locate/ijms

Mass spectrometric evidence for catenanes and rotaxanes from negative-ESI FT-ICR tandem-MS-experiments

Christoph A. Schalley[a,*], Pradyut Ghosh[1], Marianne Engeser

[a] *Kekulé-Institut für Organische Chemie und Biochemie der Universität, Gerhard-Domagk-Str. 1, D-53121 Bonn, Germany*

Received 8 January 2004; accepted 3 February 2004

Abstract

Often, it is a non-trivial task to distinguish intertwined topologies as realized in rotaxanes and catenanes from non-intertwined isomers, such as simple host–guest complexes held together by non-covalent bonds or larger mono-macrocyclic analogues. This article discusses in detail the collision-induced fragmentations of the anions of catenanes, rotaxanes, and analogous compounds bearing tetralactam macrocycles. With these experiments, it is possible to distinguish intertwined from non-intertwined complexes through differences in the fragmentation pattern.

Keywords: Supramolecular chemistry; Non-covalent complexes; Macrocycles; Catenanes; Rotaxanes; Knots; Mass spectrometry; Collision-induced dissociation

1. Introduction

Intertwined molecules, such as catenanes, rotaxanes, and knots [1–5], are currently under intense investigation by many groups due to their potential in molecular machinery (for a review, see Refs. [6,7]). Also, the design of template effects for efficient threading of one component through the other has been a focus in recent research [8–10]. An efficient synthesis of these compounds necessarily relies on precise analytical protocols for examining the topology. Recently, we have shown [11] that it is possible to distinguish catenanes, i.e., two mechanically interlocked macrocycles, from topological isomers, such as a mono-macrocycle of the same elemental composition, through their fragmentation behavior in tandem-MS-experiments [12,13]. Such analytical methods are important for the synthetic chemist, because it is not always easy to gather unambiguous evidence for the intertwined nature since the building blocks of the different isomers are the same, and thus give similar NMR spectra.

A similar difficulty arises for rotaxanes, which consist of an axle threaded into a macrocycle. In order to prevent deslippage, two bulky stopper groups are attached to the ends of the axle, thus trapping the wheel mechanically on the axle. However, the analytical problem to solve is not only to distinguish the rotaxane from other covalent isomers. Rather, non-threaded complexes of axle and wheel held together by weak non-covalent forces may be formed from which a rotaxane must become distinguishable for an unambiguous analytical characterization.

Since some of the mechanically intertwined compounds can easily be ionized as cations by attaching, for example, a proton, or a sodium ion, others, however, are more suitably examined in the form of their anions formed through deprotonation, the present study extends our previous work into the negative mode. In particular, the rotaxanes investigated here, which have not been included in the earlier work, can easily be deprotonated. As we will see, the mass spectrometric experiments with the corresponding anions provide conclusive evidence for the rotaxane structure, while the protonated analogues will likely undergo fragmentations unspecific with respect to their structure.

The compounds under study here (Chart 1) are related to each other through their common building blocks. In order to get a more complete picture, we include a series of 10 differently substituted tetralactam macrocycles (**1**–**10**) [14–17]. Some of them may be deprotonated at one of their amide bonds, others bear a phenolic OH group so that it should be

* Corresponding author. Tel.: +49-228735784; fax: +49-228735662.
E-mail address: c.schalley@uni-bonn.de (C.A. Schalley).
[1] Present address: Central Salt & Marine Chemicals Research Institute, G.B. Marg, Bhavnagar 364 002, India.

1387-3806/$ – see front matter © 2004 Elsevier B.V. All rights reserved.
doi:10.1016/j.ijms.2004.02.003

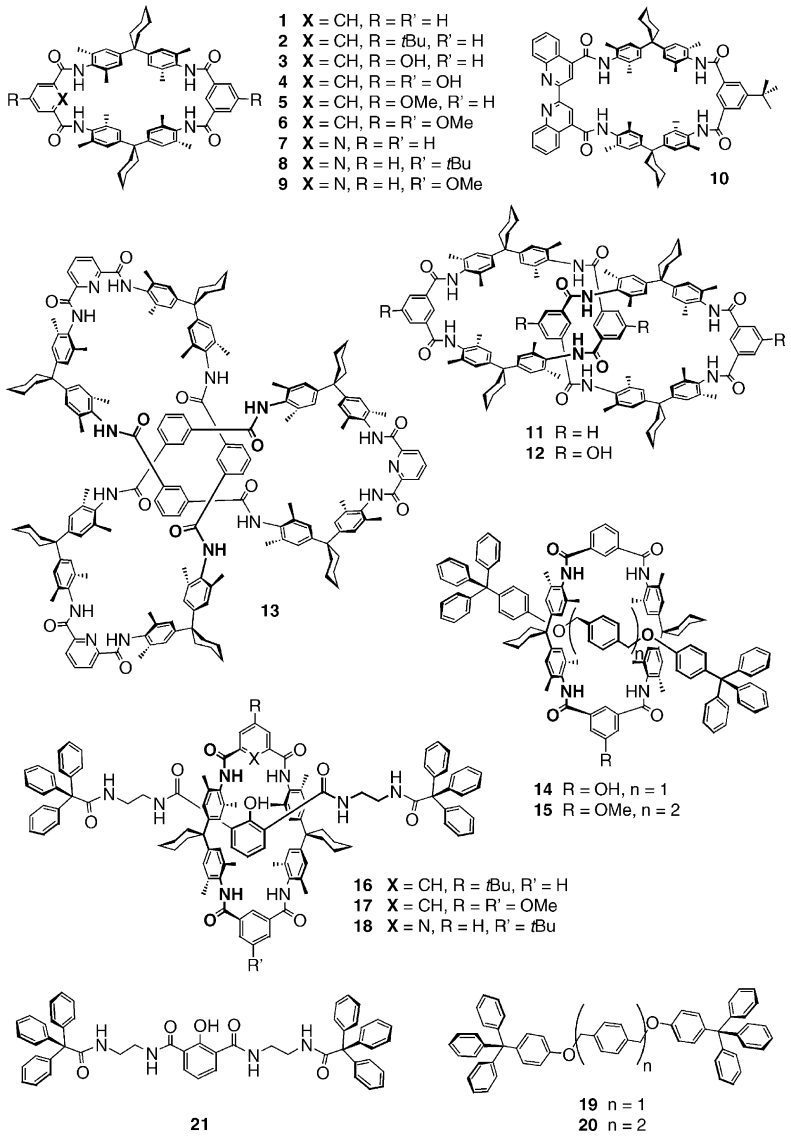

Chart 1. Structures under study here involve a series of differently substituted tetralactam macrocycles (**1**–**10**), two catenanes (**11** and **12**), the trefoil amide knot **13**, and five different rotaxanes (**14**–**18**). The axles **19**–**21** serve as control compounds.

possible to examine them as anions in the negative mode of the mass spectrometer. Their protonated analogues have already been investigated [11]. Thus, it should be interesting to compare the behavior of the macrocycles, catenanes, rotaxanes, and the knot with respect to their charge state and to examine whether the topological conclusions drawn hold true also for the negatively charged species. Two catenanes **11** and **12** were chosen, one which would be deprotonated at one of the amide bonds and one which could lose a proton from a phenol OH group. A comparison of these two structures might provide some information about the importance of the location of the negative charge for the fragmentation reactions. The largest structure is the trefoil dodecaamide knot **13**, which in contrast to the catenanes is a mono-macrocycle, although it has an intertwined topology [18,19]. Finally, the rotaxanes **14**–**18** [20–22] are included here with stopper groups large enough to prevent deslippage even at higher internal energies [23–25]. The axles **19**–**21** serve for comparison and are needed to prepare mixtures of axle and wheel in order to be able to investigate the behavior of non-covalent complexes of these two compounds.

2. Experimental

2.1. Syntheses

The syntheses, the purification, and the characterization of all compounds used in this study have been described before [14,15,17,18,20–22,26,27]. The *N*-deuterated macrocycle D_4-**1** was prepared by stirring **1** in deuterated methanol/dichloromethane 9:1 for 48 h. An ^{1}H NMR

spectrum and the parent ion region in the ESI mass spectra confirm the exchange of nearly all amide protons against deuterium (>96% of all NH protons exchanged).

2.2. Tandem-mass-spectrometric experiments

ESI mass spectra and MS/MS spectra were recorded on a Bruker APEX IV Fourier-transform ion cyclotron resonance (FT-ICR) mass spectrometer with an Apollo electrospray ion source equipped with an off-axis 70° spray needle. Typically, methanol (*O*-deuterated methanol for D_4-**1**) served as the spray solvent and 30 μM solutions of the analytes were used. When solubility in methanol was too low, dichloromethane was added in amounts as small as possible. Analyte solutions were introduced into the ion source with a syringe pump (Cole-Palmers Instruments, Series 74900) at flow rates of approximately 3–4 μl/min. Ion transfer into the first of three differential pump stages in the ion source occurred through a glass capillary with 0.5 mm inner diameter and nickel coatings at both ends. Ionization parameters—some with a significant effect on signal intensities—were adjusted as follows: capillary voltage: +4.1 to +4.4 kV; endplate voltage: +2.8 to +3.5 kV; capexit voltage: −200 to −300 V; skimmer voltages: −8 to −12 V; temperature of drying gas: 230–250 °C. The flow of the drying gas was kept in a medium range (ca. 20 psi), while the flow of the nebulizer gas was rather low (ca. 5 psi). With the gas flows and the capexit voltage, the ratio of $[M-H]^-$ to $[M+Cl]^-$ ions can be changed over a wide range. Also, they are important parameters for the optimization of the intensities of non-covalent complexes. The ions were accumulated in the instruments hexapole for 4 s, introduced into the FT-ICR cell which was operated at pressures below 10^{-10} mbar and detected by a standard excitation and detection sequence. For each measurement 16–128 scans were averaged to improve the signal-to-noise ratio.

For MS/MS experiments, the whole isotope pattern of the ion of interest was isolated by applying correlated sweeps, followed by shots to remove the higher isotopes. In particular, for the higher mass ions such as the deprotonated knot, the isolation required some care in order to maintain signal intensities during the isolation procedure, but still it was possible for all compounds under study to isolate only the first peak of the isotope pattern. After isolation, argon was introduced into the ICR cell through a pulsed valve at a pressure of approximately 10^{-8} mbar The ions were accelerated by a standard excitation protocol and detected after a 2s-pumping delay. A sequence of several different spectra was recorded at different excitation pulse attenuations in order to get at least a rough and qualitative idea of the effects of different collision energies.

3. Results and discussion

3.1. ESI mass spectra of macrocycles, catenanes, and the knot

Fig. 1 shows the negative-ESI mass spectra of macrocycle **1** and catenane **11**. These compounds may suffice as representative examples for the other macrocycles, catenanes and knot **13**, for which analogous observations have been made. Singly charged ions are generated by deprotonation of the molecules. Alternatively, chloride complexes are formed from background chloride, which likely stems from the synthesis in which acid chlorides are used. The relative abundances of these two ions can be varied much through the ionization conditions (see above). The spectra shown in Fig. 1 correspond to conditions optimized for the intensities of the deprotonated species. If desired, the signals for the chloride complexes can easily be made the base peaks just by changing the ionization conditions. In the spectra of

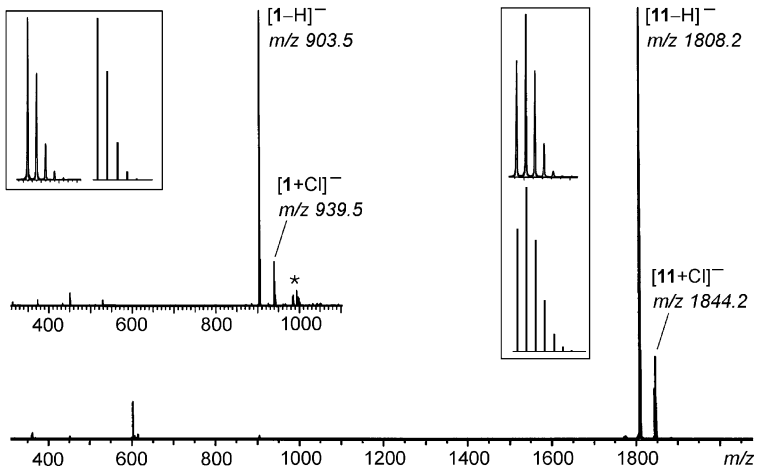

Fig. 1. Negative-ESI mass spectra of 30 μM methanol solutions of macrocycle **1** (top) and catenane **11** (bottom). The insets show the experimental isotope patterns and those calculated on the basis of natural abundances. The asterisk denotes complexes of macrocycle **1** and salt clusters, e.g., $[\mathbf{1}+NaCl-H]^-$ and $[\mathbf{1}+NaCl_2]^-$.

the macrocycles with their open cavity, signals are observed for complexes with salt clusters, e.g., $[\mathbf{1} - H + NaCl]^-$, $[\mathbf{1} + NaCl_2]^-$, $[\mathbf{1} - H + Na_2Cl_2]^-$, etc. Since no complexes with these salt clusters are observed in the spectra of the rotaxanes, the catenanes, or the knot, one might conclude that these salt clusters can easily be accommodated within the cavity of the macrocycles. In all species in which the cavity is already occupied, there is seemingly no room for these clusters and only a chloride can be attached by a hydrogen bond to an amide group at the periphery.

The identity of the species under study is confirmed (i) by the correct *m*/*z* value which deviates from the calculated exact mass by approximately 3–5 ppm and (ii) by the isotope patterns which are in good agreement with those calculated on the basis of natural abundances (insets in Fig. 1). With the resolution provided by an FT-ICR instrument, all isotope patterns are base-line resolved and can thus be easily analyzed. No doubly charged dimers are observed which would appear in the isotope patterns with a spacing of half a mass unit.

Finally, it should be noted that the mass spectra of macrocycles with phenolic OH groups, such as **3** or **4**, and those without, e.g., **1** or **2**, do not differ significantly. Similar patterns of deprotonated ions and chloride or salt complexes are found. The same holds true for the pyridine-containing macrocycles **7**–**10** and the two catenanes **11** and **12**.

3.2. Collision-induced decay of macrocycles *1*–*6*

Since all macrocycles **1**–**6** behave analogously in the collision-induced decay (CID) experiments irrespective of the presence of a phenolic OH group, we restrict the discussion to the fragmentation pattern of macrocycle **1** (Fig. 2). The four spectra shown in Fig. 2 are recorded at different collision energies and the fragment observed at the lowest collision energies is the loss of a water molecule. Upon increasing the collision energies several series of fragments arise:

(i) The first series of most prominent fragments correspond to up to four consecutive water losses. All four amide oxygen atoms must be involved in these reactions. Most likely, the amide protons are also involved, but since there are only three of them in the anion $[\mathbf{1} - H]^-$, five more hydrogen atoms are needed from another source within the molecule to account for all four water molecules. In order to get insight into which protons take part in the water losses, the deuterated analogue D_4-**1** was examined (inset in Fig. 2). However, from the parent ion $[D_4\text{-}\mathbf{1}\text{-}D]^-$ mostly H_2O is expelled accompanied by a less intense HDO loss. An analogous series of water losses has also been observed for the protonated, cationic macrocycle $[\mathbf{1} + H]^+$ and deuteration of the amide groups led to the exact same result [11]. Seemingly, there is an exchange mechanism leading to scrambling of the amide protons which is independent on the charge state. The most likely origins for the exchanged hydrogen atoms as well as those involved in the water losses in addition to the amide protons are the methyl groups in the vicinity to the amide group, because they are located at a benzylic position. Any radical, cation, or anion formed as an intermediate here would be stabilized to some extent by the aromatic ring to which the methyl groups are attached. A plausible, but speculative mechanism for the water loss is depicted in Scheme 1. It should be noted that this mechanism would not require any scrambling prior to the loss of water in order to explain that H_2O and HDO are lost. However, all other fragments discussed below suffer from a distribution of the deuterium atoms so that at least a partial scrambling must take place.

(ii) A less intense fragment is found at Δm 43.0042 Da below the parent ion also followed by up to three consecutive water losses. One might consider an expulsion of a C_3H_7 fragment (43.0548 Da) from one of the cyclohexyl side chains as a rationalization of this

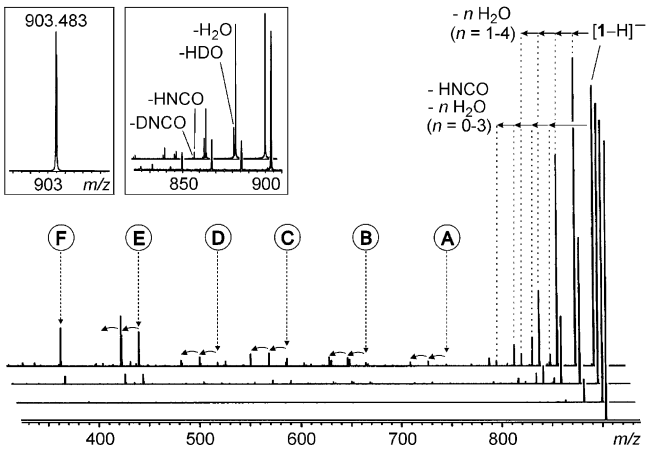

Fig. 2. MS/MS spectra of $[\mathbf{1} - H]^-$ when collided with argon at collision energies that increase from the front (no collisions, directly after isolation) to the back (ca. two thirds of the parent decomposed). The labels A to F indicate fragmentation reactions as shown in Scheme 2. Small curved arrows indicate water losses either preceding of following these fragmentations. The left inset shows the isotope pattern region after isolation. The right inset compares the water loss region of CID spectra of $[\mathbf{1} - H]^-$ and deuterium labeled $[D_4\text{-}\mathbf{1}\text{-}D]^-$ after exchange of the four amide protons in MeOD.

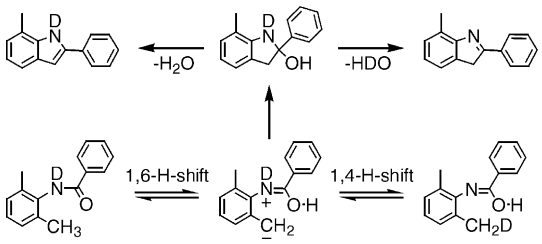

Scheme 1. Potential mechanism for the loss of water, including a pathway that rationalizes a partial scrambling of the amide and methyl hydrogen atoms.

signal, but that would not be consistent with the measured mass difference. Similar arguments apply to other neutral fragments, such as C_2H_3O (43.0184 Da), C_2H_5N (43.0422 Da), or CH_3N_2 (43.0296 Da), that in addition would be rather difficult to explain in mechanistic terms. The only fragment to which the experimental mass difference fits is HNCO (43.0058 Da). Again, the amide-deuterated parent ion yield both HNCO and DNCO as fragments in line with the assumption that the amide-centered deuterium atoms exchange with the methyl hydrogen atoms.

(iii) Finally, a series of different fragments are generated through the cleavage of two distant bonds within the macrocycle (Scheme 2). As observed for the protonated macrocycles [11], the benzylic bonds next to the cyclohexane rings can be cleaved easily. The other prominent cleavage pathway is a formal 1,2-elimination at the amide group converting it to an isocyanate. We will come across this type of bond cleavage again below and it turns out that it is quite a general reaction for the anions of the macrocycles, catenanes, and the knot. Again, all the fragments shown in Scheme 2 can be preceded or followed by water losses. The loss of an HNCO fragment as discussed above may point to a stepwise reaction sequence, in which first the bond between the carbonyl group and the aromatic ring of the isophthalic carboxamide is broken. In the next step, either a proton transfer from the amide group occurs or a second bond is broken liberating the HNCO fragment.

The fragmentation reactions discussed so far are surely quite energy demanding. This is confirmed by the finding that other, more common and more favorable reaction channels are found for the fragmentations of the rotaxanes (see below). It would require much more experimental effort to analyze the mechanisms in detail through extensive isotopic labeling and the examination of model compounds. However, since the aim of this work is to distinguish macrocycles from catenanes and rotaxanes from weakly bound non-covalent complexes, we will not go into further detail here.

3.3. Collision-induced decay of pyridine-containing macrocycles *7–10*

The pyridine- and biquinoline-containing macrocycles **7**–**10** behave somewhat differently and **7** and **10** will be discussed here as representatives for this series (Fig. 3). Macrocycles **7** and **10** again show the consecutive losses of water and the expulsion of HNCO as observed for **1**–**6**. However, isocyanate formation seems to be favored next to the pyridine ring. Macrocycle **7** loses a pyridine, while no expulsion of benzene was observed for its analogue **1**. Similarly, **10** liberates a biquinoline molecule. At low-collision energies, the products of this fragmentation reaction appear first, and thus it is even more favorable than the first water loss from **10**. The biquinoline loss is interesting, because the bond to be cleaved is located in *para*-position with respect to the pyridine nitrogen atoms. This suggests that the pyridine nitrogen not necessarily acts as an internal base promoting the reaction, but can also be turned away from the amide protons without hampering the fragmentation in its course. The other fragments can be categorized as shown in Scheme 2. It should be noted that both **7** and **10** have

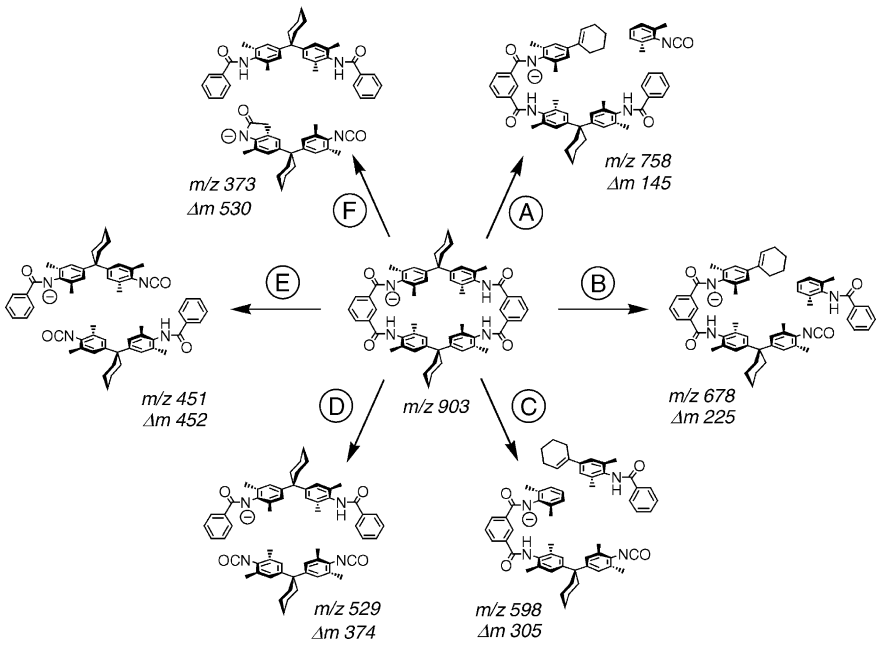

Scheme 2. Collision-induced fragmentation reactions of deprotonated **1**. Note that the exact structure of the fragments is not known, and thus the structures shown should be considered as formal representations of the ions which might have rearranged. Also, note that the fragmentations depicted here all are high-energy processes.

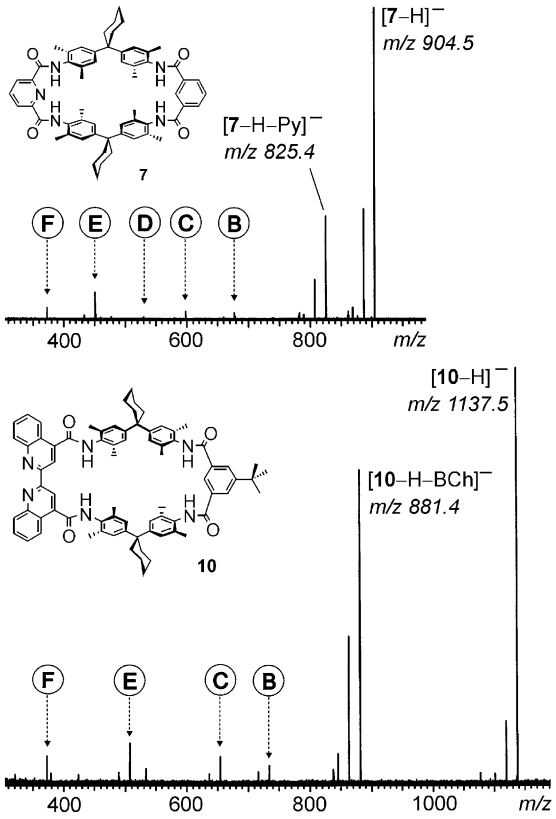

Fig. 3. MS/MS spectra of $[\mathbf{7}-H]^-$ and $[\mathbf{10}-H]^-$ when collided with argon. Most fragmentations can be rationalized by pathways analogous to those found for $[\mathbf{1}-H]^-$ (labeled B to F as in Fig. 2 and Scheme 1). Note that the *m*/*z* values shift through substitution and that some processes appear twice due to the lower symmetry in **7** and **10** as compared to **1**. In addition, losses of pyridine and bisquinoline, respectively, are observed.

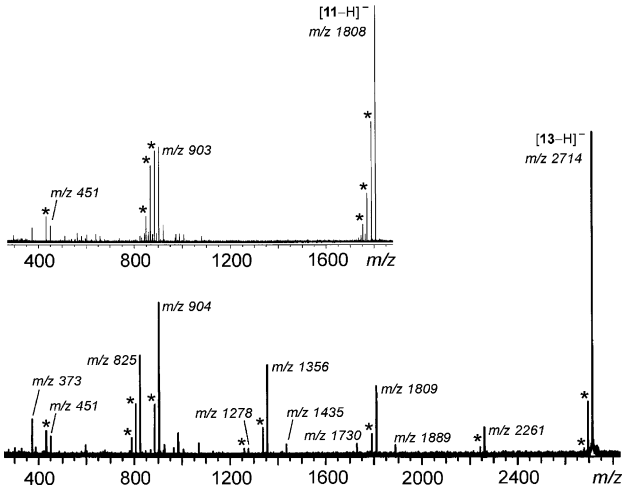

Fig. 4. (Top) MS/MS spectrum of catenane $[\mathbf{11}-H]^-$. Ring cleavage and loss of one of the wheels competes with a series of water losses as observed for macrocycle **1** (Fig. 2). (Bottom) MS/MS spectrum of knot $[\mathbf{13}-H]^-$ after collisions with argon. The series of fragments observed is shown in Scheme 2. Asterisks indicate water losses from the next larger ion.

a lower symmetry as compared to **1** so that some of the processes lead to two signals depending on which of the sides retains the negative charge. For example, two ions at *m*/*z* 451 and at *m*/*z* 452 are formed from **7** via decomposition channel **D**. The ion at *m*/*z* 451 is identical with that shown in Scheme 2 and the pyridine moiety is incorporated in the neutral fragment. Instead, the pyridine is retained in the ion at *m*/*z* 452. Similar arguments apply to the other fragmentation pathways.

*3.4. Collision-induced decay of catenanes **11** and **12** and knot **13***

Let us start with discussing the decomposition behavior of the trefoil knot **13**. Like for the other species discussed so far, water losses are observed in the CID mass spectrum of **13** (Fig. 4). However, more importantly, the knot is a mono-macrocycle, and thus two bonds need to be broken in order to obtain fragments analogous to the processes depicted in Scheme 2. Upon collisional activation, ring cleavage occurs giving rise to an extended, linear structure as shown in Scheme 3. Then, isocyanate-generating fragmentation should be possible at any of the amide groups along the chain. This is indeed observed with only two exceptions out of eleven possible cleavage sites (Fig. 4 and Scheme 3). In these two cases, the ion intensities may just be too low to be seen in the spectrum. Four signals are more prominent than the others and appear at almost regular distances: *m*/*z* 2261 (Δm 453 from the parent at *m*/*z* 2714), *m*/*z* 1809 (Δm 452 from the ion at *m*/*z* 2261), *m*/*z* 1356 (Δm 453 from the ion at *m*/*z* 1809), and *m*/*z* 904 (Δm 452 from the ion at *m*/*z* 1356). The alternation of Δm 453 and Δm 452 is due to the presence of a pyridine in the first segment of the chain, of an isophthalic dicarboxamide in the second segment, of a pyridine in the third segment of the chain, and so forth. Consequently, the sequence information is reflected in the fragmentation pattern. The fact that no signal is observed at *m*/*z* 2262, which would correspond to the analogous ring cleavage reaction within an isophthalic dicarboxamide moiety, indicates ring cleavage and isocyanate formation to be favored next to the pyridine rings in agreement with the observation of prominent pyridine and biquinoline losses from **7** and **10**. Thus, the first ring cleavage specifically occurs at this position.

Catenanes **11** and **12** behave differently in one important aspect: If one of its wheels is cleaved, the second wheel can deslip even if only one covalent bond is broken. This is reflected in the absence of any signal at *m*/*z* 1356 which would correspond to the loss of half a wheel. While none of the mono-macrocycles **1**–**6** nor knot **13** shows any strong preference for a particular second bond to be broken after the first ring cleavage reaction, the catenane has such a preference for losing one complete wheel. This can only be understood taking into account the particular topology of a catenane. For a mono-macrocycle twice the size of **1**, and thus isobaric to catenane **11**, a series of fragments similar to that of the

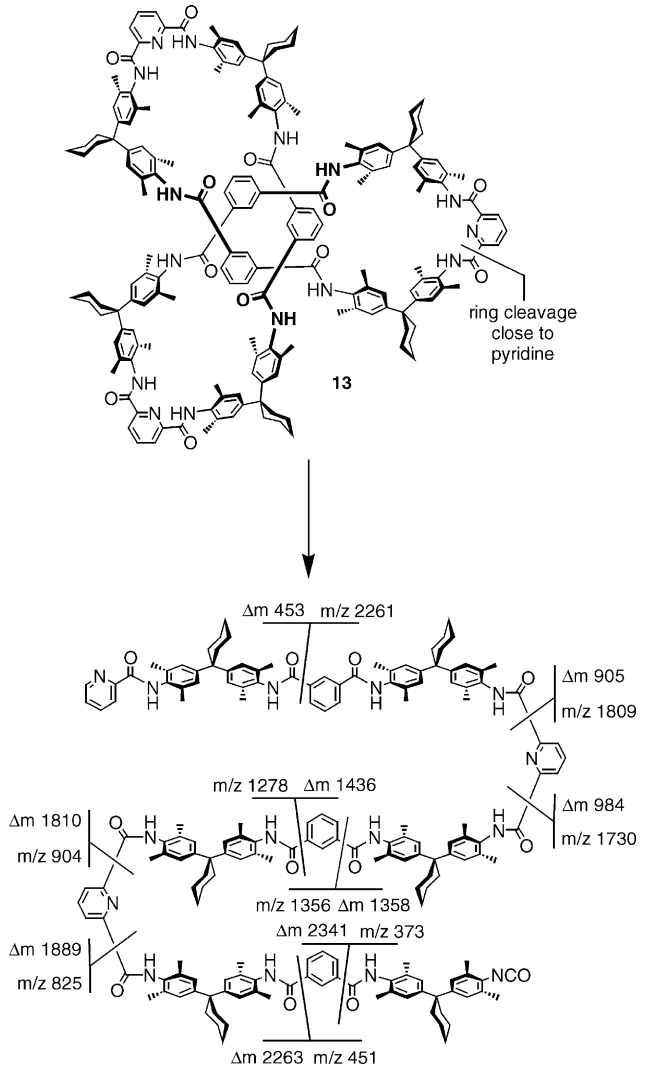

Scheme 3. Collision-induced fragmentation reactions of deprotonated knot **13**. After a first ring cleavage that occurs close to one of the pyridine units, the chain fragments as indicated. Note that the fragmentations do not correspond to simple bond cleavages, but that each reaction also involves transfer of the amide hydrogen atom to the aromatic ring to finally yield an isocyanate.

knot would be expected. Consequently, the CID spectra of the anions under study allow to distinguish a catenane from a mono-macrocyclic molecule. The arguments which apply for the negative mode similarly hold true for the protonated species [11].

One question remains: When it is possible to distinguish a catenane from a mono-macrocycle of the same elemental composition, because in the fragmentation reactions one complete wheel is lost, should not one expect a non-intertwined dimer complex to behave similarly? How can one make sure that such a complex is not mistaken for a catenane? In order to study such a complex, macrocycle **1** was used and the ionization conditions varied for maximum intensity of a dimer $[\mathbf{1}_2 - \mathrm{H}]^-$. However, we have not been able to generate intensities sufficiently large for MS/MS experiments. Under the conditions that were used for ionization of the catenane, no such complex formed at all. Consequently, $[\mathbf{1}_2 - \mathrm{H}]^-$ can be ruled out as a potential structure for the catenane ion, although under milder conditions a very tiny signal could be observed (<2% of the deprotonated macrocycle $[\mathbf{1} - \mathrm{H}]^-$).

3.5. ESI mass spectra of rotaxanes *14–18*

The rotaxanes fall in two groups. Two of them, i.e., **14** and **15**, bear an axle which unlikely carries the negative charge due to a lack of suitable functional groups. It should be much easier to deprotonate the wheel at the phenolic OH group in **14** or one of the amide groups of **15** so that the charge would reside on the wheel rather the axle. Instead, axle **21** incorporated in rotaxanes **16**–**18** is likely to carry the charge of their anions, since it contains an easy to deprotonate phenolic OH group. Another important difference is that axles **19** and **20** do not have any groups that are prone to forming strong hydrogen bonds with any of the macrocycles, while the phenolate formed upon deprotonation of **21** is capable of strong hydrogen bonding to two amide groups of the macrocycles. In dichloromethane, a binding constant of $K > 10^5\,\mathrm{M}^{-1}$ was determined The strong binding of phenolates and other anions to tetralactam macrocycles in solution has been utilized for designing template effects for efficient rotaxane synthesis [20–22,28–33]. In the gas phase, one might expect the binding to be even stronger because there is no competition with the solvent anymore.

These differences between the two types of rotaxanes are already reflected in the negative-ESI mass spectra. While rotaxanes **14** and **15** give rise to intense signals for the corresponding anions, no signal is observed for axle–wheel complexes $[\mathbf{19}\cdot\mathbf{3}-\mathrm{H}]^-$ or $[\mathbf{20}\cdot\mathbf{5}-\mathrm{H}]^-$ even under mild ionization conditions. Consequently, such complexes can be ruled out as structures for **14** and **15**, respectively. In marked contrast, axle **21** forms complexes with macrocycles such as **2**, **6**, and **8** in its deprotonated form which are strong enough in intensity for performing MS/MS experiments. Fig. 5 compares the ESI mass spectra of rotaxane $[\mathbf{18} - \mathrm{H}]^-$ (top) and the corresponding complex $[\mathbf{21}\cdot\mathbf{8} - \mathrm{H}]^-$ (bottom) obtained under exactly the same ionization conditions. The difference is obvious. Not only is the rotaxane much stronger in intensity, its spectrum is also free of signals that would correspond to the free axle $[\mathbf{21} - \mathrm{H}]^-$ and the free wheel $[\mathbf{8}-\mathrm{H}]^-$. In contrast, the intensity of the signal for complex $[\mathbf{21}\cdot\mathbf{8}-\mathrm{H}]^-$ is low as compared to the signals for the deprotonated axle and the macrocycle. As above, the experimental *m*/*z* values and the isotope patterns are in excellent agreement with those calculated. Rotaxanes **16** and **17** give the similar result. For the discussion here, **18** was chosen as example, because it bears pyridine wheel **8**, which is more easily cleaved than its analogues **2** and **6** according to the results reported above. Thus, one might have expected to observe a signal for the free axle in its spectrum rather than in those of **16** and **17**.

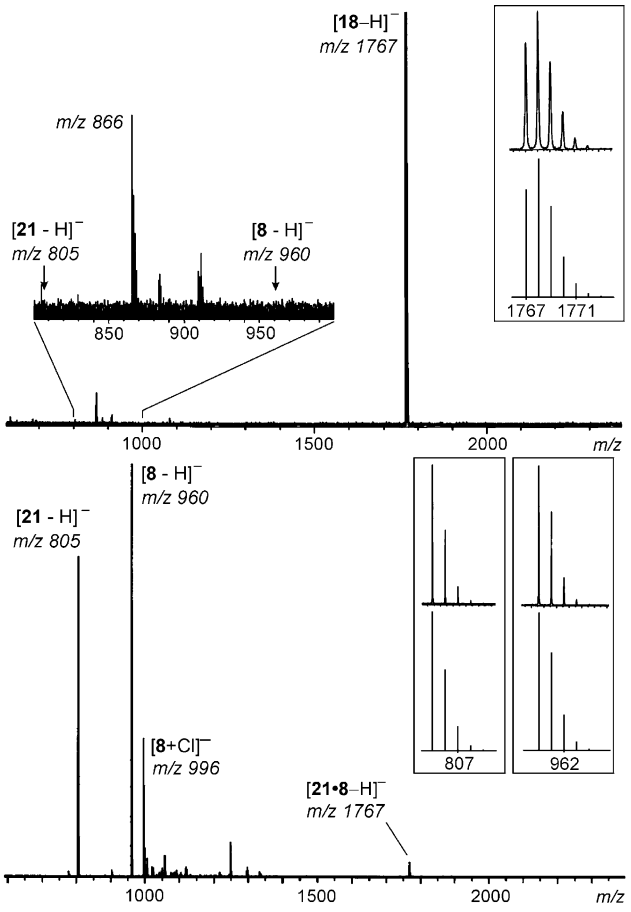

Fig. 5. Negative-ESI mass spectra of 30 μM methanol solutions of rotaxane **18** (top) and a mixture of its components, i.e., axle **21** and macrocycle **8** (bottom) obtained under the very same conditions. Note that the rotaxane spectrum does not show any signal for axle or wheel (see the enlarged part of the spectrum of *m/z* 800–1000), while these are prominent in the spectrum of the mixture. The insets show the experimental and calculated isotope patterns of the rotaxane (top) and axle and wheel (bottom).

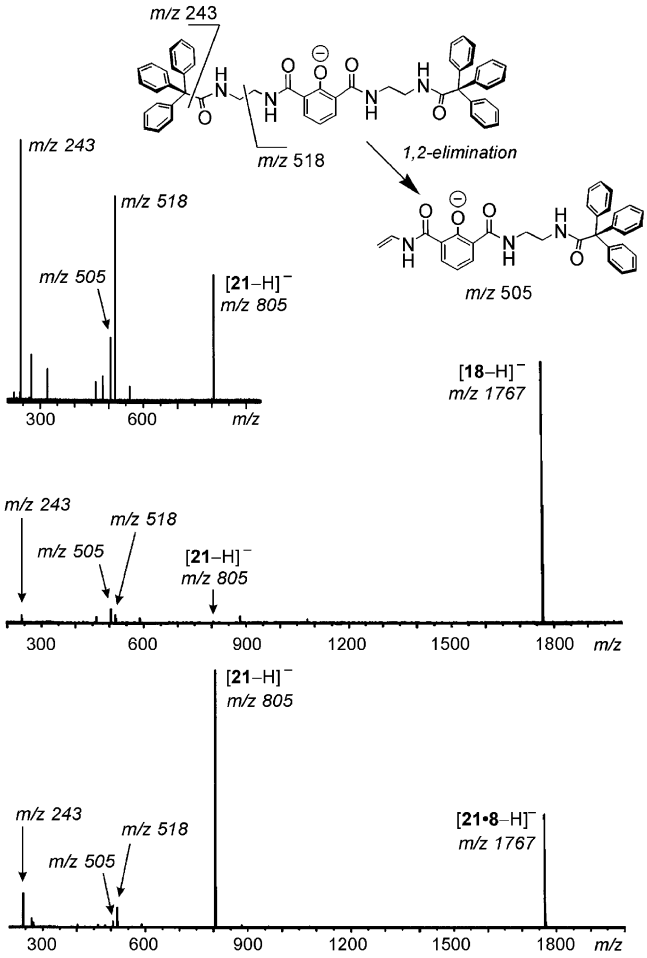

Fig. 6. MS/MS spectra of axle [**21**−H]⁻, rotaxane [**18** − H]⁻, and axle–wheel complex [**21**·**8** − H]⁻ when collided with argon. Note that no signal is observed for the deprotonated axle in the rotaxane spectrum, while it is prominent among the products generated from the axle–wheel complex. The structures (top) indicate the fragmentations pathways of the axle [**21** − H]⁻ leading to the major products.

*3.6. Collision-induced decay of rotaxanes **14–18** and non-threaded analogues*

For an analysis of the CID spectra of rotaxanes **16**–**18** it is useful to look at the spectra of the deprotonated axle **21** first (Fig. 6, top). Characteristic fragments from [**21** − H]⁻ are (i) the triphenylmethyl anion at *m/z* 243, (ii) the product of a bond cleavage reaction within one of the ethylene diamine spacers at *m/z* 518, and (iii) a product generated by a 1,2-elimination within that spacer at *m/z* 505.

When rotaxane [**18**−H]⁻ is isolated and collided with argon (Fig. 6, center), only fragments of the axle are observed as products. The typical decomposition products of the tetralactam macrocycle, i.e., water losses, the expulsion of HNCO, or ring cleavages are not observed. This indicates that the decay of the axle is less energy demanding than that of the macrocycle. Similarly, complex [**21**·**8**−H]⁻ (Fig. 6, bottom) does not show any of these macrocycle fragments, but the intact axle as major product and again fragments of the axle (which are likely consecutive decomposition products from the axle anion at *m/z* 805). Of course, for a non-covalently bound complex in which the two components are held together by weak interactions, one would not expect such energy-demanding fragmentations to compete, and thus this result is not unexpected. However, most important for the question whether **18** is a rotaxane or an axle–wheel complex is one decisive difference in the CID spectra of [**18** − H]⁻ and [**21**·**8**−H]⁻. From [**18** − H]⁻ hardly any free axle is formed as a product, while it represents the major product upon collisional activation of [**21**·**8** − H]⁻. This difference alone clearly excludes the structure of a non-threaded complex for [**18** − H]⁻. We can easily understand these findings, when considering that loss of the macrocycle is straightforward for a hydrogen-bonded axle–wheel complex with the negative charge located on the axle. In contrast, the rotaxane bears an additional mechanical bond holding the wheel on the axle so that it cannot decompose without breaking a

covalent bond within the axle or the wheel, even when it has enough internal energy to break any non-covalent forces which may operate between its components. Since the rupture of a covalent bond of the axle is more favorable in energy, a neutral fragment of the axle is lost together with the wheel and only fragments of the axle are observed as products.

Another argument supporting this line of reasoning is the fact that under exactly the same conditions, approximately 85% of the rotaxane $[\mathbf{18} - H]^-$ are still intact, while more than two thirds of the non-covalent complex $[\mathbf{21}\cdot\mathbf{8} - H]^-$ are already destroyed. Not surprisingly, the decomposition of the rotaxane through covalent bond cleavage requires more energy than breaking the hydrogen bonds between axle and wheel in $[\mathbf{21}\cdot\mathbf{8} - H]^-$.

4. Conclusions

The most important conclusion from the experiments presented here is that mass spectrometry, carefully used, may provide more than just an exact mass. Beyond its 'normal' use for mass analysis, it gives structural information [34–36], even for such large and floppy molecules as catenanes and rotaxanes. Of course, control experiments with isomeric structures should be done whenever possible. If this is taken care of, mass spectrometry is an extremely helpful tool for the synthetic supramolecular chemist.

Besides that we have analyzed the fragmentation behavior of tetralactam macrocycles, the corresponding catenanes and rotaxanes and of the trefoil amide knot in some detail. A general pattern evolved which includes series of water losses, the expulsion of HNCO and several ring cleavage reactions which likely generate isocyanates upon high-energy collisions. This pattern does not apply to the rotaxanes under study, because here, the energetically more favorable fragmentation reactions of the axles prevailed and no decomposition of the wheel is observed. Among the compounds utilized for this study have been those which could be easily deprotonated at a phenolic OH group and those that could not and rather had to be deprotonated at one of the incorporated amide groups. No significant differences have been observed between these. Consequently, for the energy-demanding processes occurring, the location of the charge does not matter much.

Finally, with the exception of the rotaxanes, there is a striking similarity in the fragmentation reactions of the anions in this study and the corresponding protonated species which have been studied earlier [11]. The same series of water losses occur in both charge states. Even the isotopic scrambling is observed for both cases. One may speculate that this points to reactions that are not induced by the positive or negative charge, but would also occur in a neutral compound. To clarify this issue, much more experimental effort would be necessary and for the time being we cannot provide the final solution.

In summary, mass spectrometry is a powerful tool to confirm and deduce the topology of supramolecular, intertwined molecules, irrespective of their charge state.

Acknowledgements

P.G. thanks the Alexander-von-Humboldt Foundation for a postdoctoral fellowship. C.A.S. is grateful for a Heisenberg Fellowship of the Deutsche Forschungsgemeinschaft. We thank Gabriele Silva for synthesizing many of the macrocycles, catenanes, and the knot. Funding from the DFG (SFB 624) and the Fonds der Chemischen Industrie are acknowledged.

References

[1] G. Schill, Catenanes, Rotaxanes and Knots, Academic Press, New York, 1971.
[2] R. Jäger, F. Vögtle, Angew. Chem. 109 (1997) 966;
R. Jäger, F. Vögtle, Angew. Chem. Int. Ed. Engl. 36 (1997) 931.
[3] S.A. Nepogodiev, J.F. Stoddart, Chem. Rev. 98 (1998) 1959.
[4] F.M. Raymo, J.F. Stoddart, Chem. Rev. 99 (1999) 1643.
[5] J.P. Sauvage, C. Dietrich-Buchecker (Eds.), Molecular Catenanes, Rotaxanes, and Knots, Wiley-VCH, Weinheim, 1999.
[6] C.A. Schalley, K. Beizai, F. Vögtle, Acc. Chem. Res. 34 (2001) 465 (also, see the other reviews in this special issue on molecular machines).
[7] V. Balzani, M. Venturi, A. Credi, Molecular Machines and Devices, Wiley-VCH, Weinheim, 2003.
[8] F. Diederich, P.J. Stang (Eds.), Templated Organic Synthesis, Wiley-VCH, Weinheim, 2000.
[9] M. Kogej, P. Ghosh, C.A. Schalley, How to thread a string into the eye of a molecular needle, in: M. Harmata (Ed.), Strategies and Tactics in Organic Synthesis, Elsevier (in press).
[10] W. Reckien, C.A. Schalley, S. Peyerimhoff, F. Vögtle, J. Am. Chem. Soc. (submitted for publication).
[11] C.A. Schalley, J. Hoernschemeyer, X.-y. Li, G. Silva, P. Weis, Int. J. Mass Spectrom. 228 (2003) 373.
[12] C.A. Schalley, Int. J. Mass Spectrom. 194 (2000) 11.
[13] C.A. Schalley, Mass Spectrom. Rev. 20 (2001) 253.
[14] C.A. Hunter, J. Chem. Soc. Chem. Commun. (1991) 749.
[15] C.A. Hunter, J. Am. Chem. Soc. 114 (1992) 5303.
[16] F. Vögtle, T. Dünnwald, T. Schmidt, Acc. Chem. Res. 29 (1996) 451.
[17] X.-y. Li, J. Illigen, M. Nieger, S. Michel, C.A. Schalley, Chem. Eur. J. 9 (2003) 1332.
[18] O. Safarowsky, M. Nieger, R. Fröhlich, F. Vögtle, Angew. Chem. 112 (2000) 1699;
O. Safarowsky, M. Nieger, R. Fröhlich, F. Vögtle, Angew. Chem. Int. Ed. 39 (2000) 1616.
[19] F. Vögtle, A. Hünten, E. Vogel, S. Buschbeck, O. Safarowsky, J. Recker, A. Parham, M. Knott, W.M. Müller, U. Müller, Y. Okamoto, T. Kubota, W. Lindner, E. Francotte, S. Grimme, Angew. Chem. 113 (2001) 2534;
F. Vögtle, A. Hünten, E. Vogel, S. Buschbeck, O. Safarowsky, J. Recker, A. Parham, M. Knott, W.M. Müller, U. Müller, Y. Okamoto, T. Kubota, W. Lindner, E. Francotte, S. Grimme, Angew. Chem. Int. Ed. 40 (2001) 2468.
[20] C.A. Schalley, G. Silva, C.F. Nising, P. Linnartz, Helv. Chim. Acta 85 (2002) 1578.
[21] P. Ghosh, O. Mermagen, C.A. Schalley, Chem. Commun. (2002) 2628

[22] P. Ghosh, A. Lützen, C.A. Schalley, J. Am. Chem. Soc. (submitted for publication).
[23] A. Affeld, G.M. Hübner, C. Seel, C.A. Schalley, Eur. J. Org. Chem. (2001) 2877.
[24] T. Felder, C.A. Schalley, Angew. Chem. 115 (2003) 2360;
T. Felder, C.A. Schalley, Angew. Chem. Int. Ed. 42 (2003) 2258.
[25] P. Linnartz, S. Bitter, C.A. Schalley, Eur. J. Org. Chem. (2003) 4819.
[26] S. Ottens-Hildebrandt, S. Meier, W. Schmidt, F. Vögtle, Angew. Chem. 106 (1994) 1818;
S. Ottens-Hildebrandt, S. Meier, W. Schmidt, F. Vögtle, Angew. Chem. Int. Ed. Engl. 33 (1994) 1767.
[27] F. Vögtle, S. Meier, R. Hoss, Angew. Chem. 104 (1992) 1628;
F. Vögtle, S. Meier, R. Hoss, Angew. Chem. Int. Ed. 31 (1992) 1619.
[28] G.M. Hübner, J. Gläser, C. Seel, F. Vögtle, Angew. Chem. 111 (1999) 395;
G.M. Hübner, J. Gläser, C. Seel, F. Vögtle, Angew. Chem. Int. Ed. 38 (1999) 383.
[29] C. Reuter, W. Wienand, G.M. Hübner, C. Seel, F. Vögtle, Chem. Eur. J. 5 (1999) 2692.
[30] C. Reuter, F. Vögtle, Org. Lett. 2 (2000) 593.
[31] C. Seel, F. Vögtle, Chem. Eur. J. 6 (2000) 21.
[32] J.A. Wisner, P.D. Beer, N.G. Berry, B. Tomapatanaget, Proc. Natl. Acad. Sci. U.S.A. 99 (2002) 4983.
[33] J.A. Wisner, P.D. Beer, M.G.B. Drew, M.R. Sambrook, J. Am. Chem. Soc. 124 (2002) 12469.
[34] B.M. O'Leary, T. Szabo, N. Svenstrup, C.A. Schalley, A. Lützen, M. Schäfer, J. Rebek Jr., J. Am. Chem. Soc. 123 (2001) 11519.
[35] C.A. Schalley, T. Müller, P. Linnartz, M. Witt, M. Schäfer, A. Lützen, Chem. Eur. J. 8 (2002) 3538.
[36] H. Mansikkamäki, M. Nissinen, C.A. Schalley, K. Rissanen, New J. Chem. 27 (2003) 88.